# Optogenetic Engineering of Photoactivatable NanoCRISPR for Programmable Genome Editing

Xiaohong Chen[a,1], Yuxuan Chen[a,1], Huhu Xin[a], Tao Wan[a], Yuan Ping[a,2]

[a]College of Pharmaceutical Sciences, Zhejiang University, Hangzhou 310058, China

[b]College of Animal Science and Technology, Zhejiang A&F University, Hangzhou 311300, China

Author contributions: Y.P. conceived the project and designed experiment. X.C. performed in vitro and in vivo experiments. Y.C. synthesized and characterized polymer-coated gold materials. H.X. constructed the plasmids. T.W., H.X., and Y.P. planned and interpreted the data. Y.P. supervised the project, and wrote manuscript.

Conflict of Interest: The authors declare no conflict of interest.

[1]These authors contributed equally to this work: X.C. and Y.C.

[2]Corresponding and requests for materials should be addressed to Y.P. Email: pingy@zju.edu.cn

## Abstract

We herein report the first optogenetically activatable CRISPR/Cas9 nanosystem for programmable genome editing in the second near-infrared (NIR-II) optical window. The nanosystem, termed as NanoCRISPR, is composed of a cationic polymer-coated gold nanorod (APC) and Cas9 plasmid driven by a heat-inducible promoter. APC not only serves as a carrier for intracellular plasmid delivery, but also can harvest external NIR-II photonic energy and convert into local heat to induce the gene expression of Cas9 endonuclease. Due to high transfection activity, APC shows strong ability to induce significant level of disruption in different genome loci upon optogenetic activation. Moreover, the precise control of genome editing activity can be simply programmed by finely tuning exposure time and irradiation times in vitro and in vivo, and also enables editing at multiple time points, thus proving the sensitivity and reversibility of such an editing modality. The NIR-II optical feature of NanoCRISPR enables therapeutic genome editing at the deep tissue of the tumor-bearing mice, by which tumor growth could be effectively inhibited as a proof-of-concept therapeutic example. Importantly, this modality of optogenetic genome editing can significantly minimize the off-target effect of CRISPR/Cas9 in the most potential off-target sites. The optogenetically activatable CRISPR/Cas9 nanosystem we have developed offers a useful tool to expand the current applications of CRISPR/Cas9, and also defines a programmable genome editing strategy towards unprecedented precision and spatiotemporal specificity.

## Keywords

CRISPR/Cas9 | Gene Delivery | Spatiotemporal Specificity | Photoregulation | Off Target

## Introduction

The RNA-guided clustered, regularly interspaced, short palindromic repeats (CRISPR)-associated nuclease protein 9 (Cas9) is originally an adaptive immune defense system, by which many bacteria exploit to protect themselves from invading genetic elements (1). It has been recently harnessed as an efficient tool for genome editing in both single cells and the whole organism for a wide range of biomedical applications in biology, genetics, and medicine, etc (2, 3). In principle, the CRISPR/Cas9 is composed a single-guide RNA (sgRNA) for the identification of DNA targets and a Cas9 endonuclease that can bind and process the recognized DNA targets (4). CRISPR/Cas9-based genome editing technology offers a powerful and reliable strategy for the targeted modifications of the genome, enabling the precise perturbation of virtually any genomic sequence in living cells (2-6). Due to its genome-wide specificity and multiplexing capability, Cas9 and its variants have shown great potentials in the generation of loss-of-function animals (7, 8), the correction of genetic disorders (9, 10), functional genome screening (11-15), and the treatment of infectious diseases (16, 17). Despite of these excitements, the lack of temporal and spatial precision during editing process has severely constrained the current CRISPR/Cas9 systems from complicated and diverse genome-editing scenarios.

Furthermore, off-target activity has now become a major concern when the CRISPR/Cas9 system is exploited for therapeutic purposes.

To improve the spatiotemporal specificity of Cas9-mediated genomic manipulation, recent efforts have been dedicated to the development of inducible CRISRP/Cas9 architectures to enable the conditional control of Cas9 activity through either chemical (18-22) or optical (23-26) means. By precisely limiting the time of Cas9 function, the off-target activity is also expected to be controlled by minimizing the unwanted prolong Cas9 activity (19, 26). Chemical methods mainly refer to the regulation of endonuclease activity of Cas9 through small-molecule-triggered Cas9 binding and self-splicing inteins (19-21). Although a few examples have been illustrated for the temporal control of Cas9 activity (27-29), however, this strategy generally lacks spatial specificity and reversibility, making it difficult to be explored for in vivo studies. Furthermore, the commonly used small molecules for chemical activation, such as rapamycine (22) and doxycycline (19, 21), may induce potential cytotoxicity towards both edited and non-edited cells (30). As opposed to the chemical strategies, optical regulation of Cas9 function is more favorable in terms its non-invasiveness, spatiotemporal specificity and reversibility. In the past few years, several different photoactivatable systems have been adopted for the optical regulation of CRISPR/Cas9-based genome editing and transcriptional activation (31, 32). For example, photoactivatable Cas9 consisting of two split, deactivated Cas9 (dCas9) fragments and photoinducible dimerization domains (Magnets) was engineered to enable optogenetic control of CRISPR-Cas9 activity in human cells (26). Upon blue light irradiation, the split Cas9 was fused to Magnet domains to recover its genome editing activity, which could be simply switched off by extinguishing the irradiation. More recently, optogenetic anti-CRISPR variants comprising a powerful Cas9 inhibitor (hybrids of AcrIIA4) and a LOV2 photosensor, were engineered for the photoregulation of CRISPR-Cas9 activity (33). As the photoirradiation enabled the release of dCas9 from the optogenetic variant of AcrIIA4, the inhibited Cas9 activity could be rapidly recovered to enable genome and epigenome editing. Nevertheless, most optically controlled CRISPR/Cas9 systems reply on the photoactivation by blue light. This suggests these blue light-mediated activatable CRISPR/Cas9 systems are not only difficult for deep-tissue penetration through turbid human tissues, but also are potentially phototoxic in the realistic genome-editing applications. To address these issues, far-red light-mediated CRISPR-dCas9 device, which is built based on the bacterial photoactivatable cyclic diguanylate monophosphate (c-di-GMP) synthase BphS and the c-di-GMP-responsive hybrid transactivator, has been recently developed for the targeted epigenetic modulation both in vitro and in vivo (34). Most recently, near-infrared upconversion-activated CRISPR-Cas9 nanoparticle system have been proposed for the optical control of therapeutic gene editing towards cancer treatment (35). While above two studies revealed the infrared light is critical for the regulation of genome editing and epigenome editing in vivo, the precise CRISPR/Cas9 genome editing in a programmable, reversible manner has not been demonstrated yet, not to mention those for in vivo applications. In

addition, off-target activity induced by light-controlled editing modalities still remains elusive to date.

## Results and Discussion

In our study, the classic cetyltrimethylammonium bromide (CTAB)-mediated synthesis approach was used for the preparation of gold nanorods (38, 39), and uniform ARs with an aspect ratio of 7.1 (length = 106.4 ± 14.1 nm, width = 15.2 ± 3.3 nm) were obtained (Fig. 2A). Afterwards, biocompatible polystyrene sulfonate (PSS), which acted as an interconnecting layer, was then coated on the AR surface through the electrostatic force to form PSS-coated ARs. Subsequently, β-cyclodextrin-PEI (CP), a cationic polymer that has been well demonstrated for the efficient transfection of plasmids for both in vitro and in vivo (40-42), was assembled on the top of the PSS layer. The layer-by-layer assembly process to prepare APC was verified by zeta potential analysis (Fig. 2B), where the final product APC showed a positive surface charge. AR displayed a strong, brand absorption in the NIR-II region, with an absorption peak at ca. 1070 nm (Fig. 2C). Noticeably, the assembly of polyelectrolytes on AR merely affected the wavelength of maximum absorption. Such a NIR-II optical feature is crucial for in vivo investigations. Upon continuous laser irradiation at 1064 nm for 5 min, the temperature of APC solution quickly increased and achieved the plateau of 42 °C under a power density at 0.33 $W/cm^2$, as recorded by the infrared thermal camera (Fig. 2D). The maximum temperature generated by APC could be further adjusted to 65 °C at a power density of 1.00 $W/cm^2$. To demonstrate whether APC was able to encapsulate the plasmid encoding Cas9 and luciferase, gel electrophoresis assay was first carried out. APC could completely inhibit plasmid DNA migration at APC/plasmid weight ratio of 0.15, proving its excellent capability to condense and carry plasmid DNA for gene transfection (Fig. 2G).

To mark Cas9 expression, the two reporters EGFP and luciferase, which is also driven by HSP70 promoter, can express with Cas9 simultaneously (Fig. 2H). Therefore, we first checked the GFP expression after the intracellular delivery of APC/HSP-Cas9 complexes. As shown in Fig. 2I, very weak fluorescence generated from green fluorescence protein (GFP) was observed in the 293T cells without laser treatment, implying the low background activity. In sharp contrast, strong green fluorescence was observed after the light irradiation on the cells. Flow cytometry analysis indicated that after APC-mediated transfection and photothermal activation, the percentage of GFP-positive cells reached more than 90% under the laser irradiation, which is much higher than that from the transfection supported by Lipofectamine 2000 (Lipo, commercially available transfection agent) or PEI (non-viral ‘gold standard’ transfection agent) at 42 °C (Fig. 2J). In the meantime, Bio-TEM image indicated that APC was primarily located in the cytoplasm after the GFP expression (Fig. 2K). These results suggested that APC could not only mediate efficient transfection, but also trigger HSP70-regulated gene expression upon photothermal activation.

Based on the above optimized results, we subsequently investigated whether optogenetic control of CRISPR/Cas9 activity could be manipulated through efficient transfection and photothermal conversion by APC (Fig. 3A). First, we tested whether APC was capable of disrupt enhanced green fluorescence protein (EGFP) gene in 293T cells that stably expressed EGFP (Fig. 3B). Upon the intracellular delivery of APC/HSP-Cas9 targeting EGFP, the intensity of GFP in 293T-EGFP cells decreased significantly with the laser irradiation, suggesting the strong ability of APC to mediate the disruption of GFP gene. Nevertheless, the treatment with APC/HSP-Cas9-sgEGFP without laser irradiation had negligible knockout effects. To further validate the genome editing efficiency, we studied the intracellular delivery of HSP-Cas9 plasmid targeting different genome loci in the 293T cell line. Indels (insertion and deletion) detected by T7 Endonuclease I (T7E1) digestion assays were carried out to evaluate the efficiency of genome editing at the targeted genome sites. After the transfection and the photothermal activation, the bands from the digestion products of T7E1 distinguishing indels in the double-stranded DNA, were clearly detected from the uncut bands at the genomic locus of adeno-associated virus integration site 1 (*AAVS1*). We noted that the editing efficiency is slightly dependent on the APC concentration, with the highest indel rate of 20.1% at the APC/plasmid weight ratio of 1:2. As expected, *AAVS1* genome editing by Lipo and PEI resulted in the indel rate of 8.9% and 3.3%, respectively, both of which were lower than that of APC-mediated genome editing (Fig. 3C). Sanger sequencing confirmed indels at the targeted loci, including base deletion, insertion and substitution around the protospacer adjacent motif (PAM) (Fig. 3D). In the meantime, we further investigated whether the level of GPF expression is synchronized with the Cas9-mediated genome disruption. As expected, the level of GFP expression was well correlated with the indel rate, suggesting the level of GFP expression could well reflect and estimate the indel rate (Fig. 3E). Similarly, by screening different sequences of sgRNA (Table S2 and S3), the optimized genome editing at rhomboid family member 1 (*RHBDF1*) locus mediated by APC showed an indel rate of 14.8%, which is more efficient than that of Lipo (6.5%) (Fig. 3F). Furthermore, we examined whether the optogenetic control could likewise activate the multiplex genome editing. To this end, we delivered two plasmids, both of which encoded a single but different sgRNA construct targeting *AAVS1* and *Plk1* (polo-like kinase 1), respectively. Both genome loci showed evident degree of editing, with the indel rates of 28.8% (*AAVS1*) and 37.0% (*Plk1*) (Fig. 3 G and H). Since APC can well absorb NIR-II light that can afford deep-tissue penetration, we covered the cell culture plate with the breast chicken tissue of different thickness and investigated whether the irradiation could still activate the genome editing in the transfected cells in the presence of tissue (Fig. 3I). Though the increase of the tissue thickness impaired the genome editing activity, the indel (6.6%) could be still detectable in the presence of 12 mm of breast chicken tissue. The above data suggest that the temperature window between 39 to 42 °C is optimal for optogenetic activation of Cas9 transcription. Interestingly, such optogenetic activation also works well for dCas9-mediated transcriptional activation of exogenous genes. For example, when three plasmids (HSP-dCas9-SPH, U6-sgRNA, and miniCMV-mCheery) were co-transfected in 293T cells, only very low basal

fluorescence was observed before optogenetic activation, due to the weak ability of miniCMV to induce transcription. In sharp contrast, mCherry expression became very strong after the transcriptional activation of the heat-shock promoter, suggesting its potential towards heat-inducible transcriptional activation (Fig. 3J).

## Materials and Methods

### Materials

Sodium borohydride ($NaBH_4$), silver nitrate ($AgNO_3$), hydroquinone (HQ), Dulbecco's modified Eagle's medium (DMEM), polyethyleneimine (PEI, MW: 25k Da) and D-luciferin-K+ salt bioluminescent substrate was purchased from Sigma-Aldrich (USA). Tetrachloroauric(III) acid trihydrate ($HAuCl_4{\cdot}3H_2O$), cetyltrimethylammonium bromide (CTAB), poly(sodium 4-styrenesulfonate) (PSS, MW ~70,000 g/mol) were purchased from Aladdin (China). The cell counting kit-8 (CCK-8) was obtained from DOJINDO (Japan). Propidium iodide (PI), Calcein acetoxymethyl ester (Calcein AM), penicillin−streptomycin, phosphate-buffered saline (PBS), fetal bovine serum (FBS) and Lipofectamine 2000 (Lipo) were purchased from Thermo Fisher Scientific (USA). Cell cycle and apoptosis analysis kit were purchased from Beyotime (China). T7 endonuclease I (T7E1) enzyme was purchased from GenScript (USA). Ultrapure water was used in all experiments. Antibodies used in this project included the following: *Plk1* antibody (#4535) and anti-GAPDH (#2118) were obtained from Cell Signalling Technology (USA). 1064 nm low power NIR Laser was purchased from Fingco (China).

### Synthesis of Gold Nanorods (ARs)

ARs were synthesized using a seed-mediated growth method as previously described (38, 39) with minor modification. Briefly, the seed solution was first synthesized by adding freshly prepared 600 μL $NaBH_4$ (10 mM) into 5 mL mixture of $HAuCl_4{\cdot}3H_2O$ (0.5 mM) and CTAB (0.1 M), followed by being kept at 30 °C for 30 min to exhaust excess $NaBH_4$. The growth solution containing a mixture of 5 mL $HAuCl_4{\cdot}3H_2O$ and 5 mL CTAB (0.2 M), 120 μL $AgNO_3$ (0.1 M) and 600 μL HQ (0.1 M) were added in sequence. When the solution color turned from yellow to colorless, 320 μL seed solution was added to the growth solution. AuNRs with the desired longitudinal surface plasmon resonance (LSPR) peak were obtained after keeping the reaction mixture undisturbed in dark at 30 °C for 12 h. Finally, the ARs were collected by centrifugation at 7000 rcf for 10 min at 30 °C. The supernatant was removed and precipitate was resuspended in 2 mL 30 °C ultrapure water.

### Synthesis of APC

For the synthesis of AR-PSS, ARs were first coated with PSS by the previous reported method (65). In brief, 1 mL of AR solution (0.2 mg/mL Au) were added to 10 mL of PSS (2 mg/mL) dissolved in NaCl (1 mM) solution and stirred for 1 h at 30 °C. A centrifugation

cycle of 7000 rcf for 10 min, and the residue was re-suspended to obtain 2 mL PSS-coated AR (AR-PSS) solution. β-CD-PEI which was synthesized by our reported method (40-42) was further coated onto AR-PSS using a similar method. 1 mL of AuNR-PSS were added to 10 mL of β-CD-PEI (2 mg/mL) dispersed in NaCl (1 mM) solution and stirred for 1 h at 30 °C to obtain AR-PSS-β-CD-PEI (APC).

### Heat-inducible Cas9/dCas9 plasmids construction

To construct HSP70-Cas9-GFP-luciferase-U6-sgRNA plasmid, HSP70 promoter core sequence (66) was amplified from genomic DNA of 293T cells by PCR and inserted into pCS2-CMV-Cas9-P2A-GFP-P2A-luciferase-pA (Addgene #48138) by replacing CMV promoter through Hind III restriction site. U6-sgRNA fragment was also added to the plasmid by SalI. CMV-Cas9-GFP-luciferase plasmid was constructed by replaced HSP70 promoter with CMV promoter. Other plasmids (HSP-Cas9-U6-gRNA and HSP-Cas9-GFP-U6-gRNA) were constructed similarly using the same molecular cloning methods.

The plasmids of CRISPR-dCas9-based transcriptional activation system were constructed based on SPH system (an improved dCas9 activation system) according to the reported literature (67). In brief, for HSP-dCas9 plasmid, dCas9-10×GCN4-P2A-SPH-T2A-GFP fragment was amplified from AP111 (Addgene #107307) by PCR, and inserted into the HSP70 promoter backbone plasmid. For exogenous mCherry activation, a weak promoter miniCMV was ligated to mCherry fragment, and one dCas9 target sequence (5'-GTCCCCTCCACCCCACAGTG-3') was added upstream of miniCMV-mCherry plasmid. U6-sgRNA plasmid also contained the same target sequence. For endogenous gene activation, only U6-sgRNA targeted 5'UTR of the candidate gene was co-transfected with HSP-dCas9 plasmid. The control plasmid CMV-dCas9 was constructed based on HSP-dCas9 plasmid by replacing its promoter.

## Acknowledgments

The authors gratefully acknowledge the National Natural Science Foundation of China (81872807), Fundamental Research Funds for the Central Universities (2018XZZX001-14), and Thousand Talents Plan (Y.P.), for the financial support of this work. The authors also acknowledge Dr. D. Wu for the helpful discussion on the synthesis of gold nanorod, and S. Zhang for the help in the construction of plasmids.

### References

1. Jinek M, et al. (2012) A programmable dual-RNA-guided DNA endonuclease in adaptive bacterial immunity. *Science* 337:816–821.
2. Cox DB, Platt RJ, Zhang F (2015) Therapeutic genome editing: prospects and challenges. *Nat Med* 21:121–131.

3. Wan T, et al. (2019) Material solutions for delivery of CRISPR/Cas-based genome editing tools: current status and future outlook. *Mater Today* 2018.12.003.
4. Nishimasu H, et al. (2014) Crystal structure of Cas9 in complex with guide RNA and target DNA. *Cell* 156:935–949.
5. Wang HX, et al. (2017) CRISPR/Cas9-Based genome editing for disease modeling and therapy: challenges and opportunities for nonviral delivery. *Chem Rev* 117:9874–9906.
6. Mout R, Ray M, Lee YW, Scaletti F, Rotello VM (2017) In vivo delivery of CRISPR/Cas9 for therapeutic gene editing: progress and challenges. *Bioconjug Chem* 28:880–884.
7. Yang L, et al. (2015) Genome-wide inactivation of porcine endogenous retroviruses (PERVs). *Science* 350:1101–1104.
8. Jin L, Li J (2016) Generation of genetically modified mice using CRISPR/Cas9 and haploid embryonic stem cell systems. Zool *Res* 37:205–213.
9. Min YL, Bassel-Duby R, Olson EN (2019) CRISPR correction of duchenne muscular dystrophy. *Annu Rev Med* 70:239–255.
10. Yang Y, et al. (2016) A dual AAV system enables the Cas9-mediated correction of a metabolic liver disease in newborn mice. *Nat Nanotech* 34:334–338.
11. Shalem O, Sanjana VM, Zhang F (2015) High-throughput functional genomics using CRISPR–Cas9. *Nat Rev Genet* 16:299–311.
12. Joung J, et al. Genome-scale CRISPR-Cas9 knockout and transcriptional activation screening. *Nat Protoc* 12:828–863.
13. Ting PY, et al. (2018) Guide swap enables genome-scale pooled CRISPR–Cas9 screening in human primary cells. *Nat Methods* 15:941–946.
14. Manguso RT, et al. (2017) In vivo CRISPR screening identifies Ptpn2 as a cancer immunotherapy target. *Nature* 547:413–418.
15. Yamauchi T, et al. (2018) Genome-wide CRISPR-Cas9 screen identifies leukemia-specific dependence on a pre-mRNA metabolic pathway regulated by DCPS. *Cancer Cell* 33:386–400.
16. Liao H, et al. (2015) Use of the CRISPR/Cas9 system as an intracellular defense against HIV-1 infection in human cells. *Nat Commun* 6:6413.
17. Scoppe JA, Lebbink RJ (2017) Antiviral goes viral: harnessing CRISPR/Cas9 to combat viruses in humans. *Trends Microbiol* 25:833–850.
18. Liu KI, et al. (2016) A chemical-inducible CRISPR–Cas9 system for rapid control of genome editing. *Nat Chem Biol* 12:980–987.
19. Aubrey BJ, et al. (2015) An inducible lentiviral guide RNA platform enables the identification of tumor-essential genes and tumor-promoting mutations in vivo. *Cell Rep* 10:1422–1432.
20. Cha PH, et al. (2016) Small-molecule binding of the axin RGS domain promotes β-catenin and Ras degradation. *Nat Chem Biol* 12:593–600.
21. Dow LE, et al. (2015) Inducible in vivo genome editing with CRISPR-Cas9. *Nat Biotechnol* 33:390–394.

22. Nguyen DP, et al. (2016) Ligand-binding domains of nuclear receptors facilitate tight control of split CRISPR activity. *Nat Commun* 7:12009.
23. Zhou XX, et al. (2018) A single-chain photoswitchable CRISPR-Cas9 architecture for light-inducible gene editing and transcription. *ACS Chem Biol* 13:443–448.
24. Hemphill J, Borchardt EK, Brown K, Asokan A, Deiters A (2015) Optical control of CRISPR/Cas9 gene editing. *J Am Chem Soc* 137:5642–5645.
25. Nihongaki Y, Yamamoto S, Kawano F, Suzuki H, Sato M (2015) CRISPR/Cas9-based photoactivatable transcription system. *Chem Biol* 22:169–174.
26. Nihongaki Y, Kawano F, Nakajima T, Sato M (2015) Photoactivatable CRISPR-Cas9 for optogenetic genome editing. *Nat Biotechnol* 33:755–760.
27. Zetsche B, Volz SE, Zhang F (2015) A split-Cas9 architecture for inducible genome editing and transcription modulation. *Nat Biotechnol* 33:139–142.
28. Maji B, et al. (2016) Multidimensional chemical control of CRISPR–Cas9. *Nat Chem Biol* 13:9.
29. Davis KM, Pattanayak V, Thompson DB, Zuris JA, Liu DR (2015) Small molecule–triggered Cas9 protein with improved genome-editing specificity. *Nat Chem Biol* 11:316–318.
30. Hilton IB, Gersbach CA (2016) Chemical control for CRISPR editing. *Nat Chem Biol* 13:2.
31. Jain PK, et al. (2016) Development of light-activated CRISPR using guide RNAs with photocleavable protectors. *Angew Chem Int Ed* 55:12440–12444.
32. Polstein LR, Gersbach CA (2015) A light-inducible CRISPR-Cas9 system for control of endogenous gene activation. *Nat Chem Biol* 11:198–200.
33. Bubeck F, et al. (2018) Engineered anti-CRISPR proteins for optogenetic control of CRISPR–Cas9. *Nat Methods* 15:924–927.
34. Shao J, et al. (2018) Synthetic far-red light-mediated CRISPR-dCas9 device for inducing functional neuronal differentiation. *Proc Natl Acad Sci USA* 115:E6722–E6730.
35. Pan Y, et al. (2019) Near-infrared upconversion–activated CRISPR-Cas9 system: a remote-controlled gene editing platform. *Sci Adv* 5:eaav7199.
36. Mosser DD, Duchaine J, Massie B (1993) The DNA-binding activity of the human heat shock transcription factor is regulated in vivo by hsp70. *Mol Cell Biol* 13:5427–5438.
37. Abravaya K, Myers MP, Murphy SP, Morimoto RI (1992) The human heat shock protein hsp70 interacts with HSF, the transcription factor that regulates heat shock gene expression. *Genes Dev* 6:1153–1164.
38. Li X, et al. (2018) In vitro and in vivo photothermal cancer therapeutic effects of gold nanorods modified with mushroom β-glucan. *J Agric Food Chem* 66:4091–4098.
39. Chen Y, Zhao Y, Yoon SJ, Gambhir SS, Emelianov S (2019) Miniature gold nanorods for photoacoustic molecular imaging in the second near-infrared optical window. *Nat Nanotech* DOI: 10.1038/s41565-019-0392-3.
40. Hu Q, et al. (2015) Engineering nanoparticle-coated bacteria as oral DNA vaccines for cancer immunotherapy. *Nano Lett* 15:2732–2739.

41. Wu M, et al. (2017) Targeting ETS1 with RNAi-based supramolecular nanoassemblies for multidrug-resistant breast cancer therapy. *J Control Release* 253:110–121.
42. Zhang Z, et al. (2018) Cationic polymer-mediated CRISPR/Cas9 plasmid delivery for genome editing. *Macromol Rapid Commun* 1800068.

## Figures and Schemes

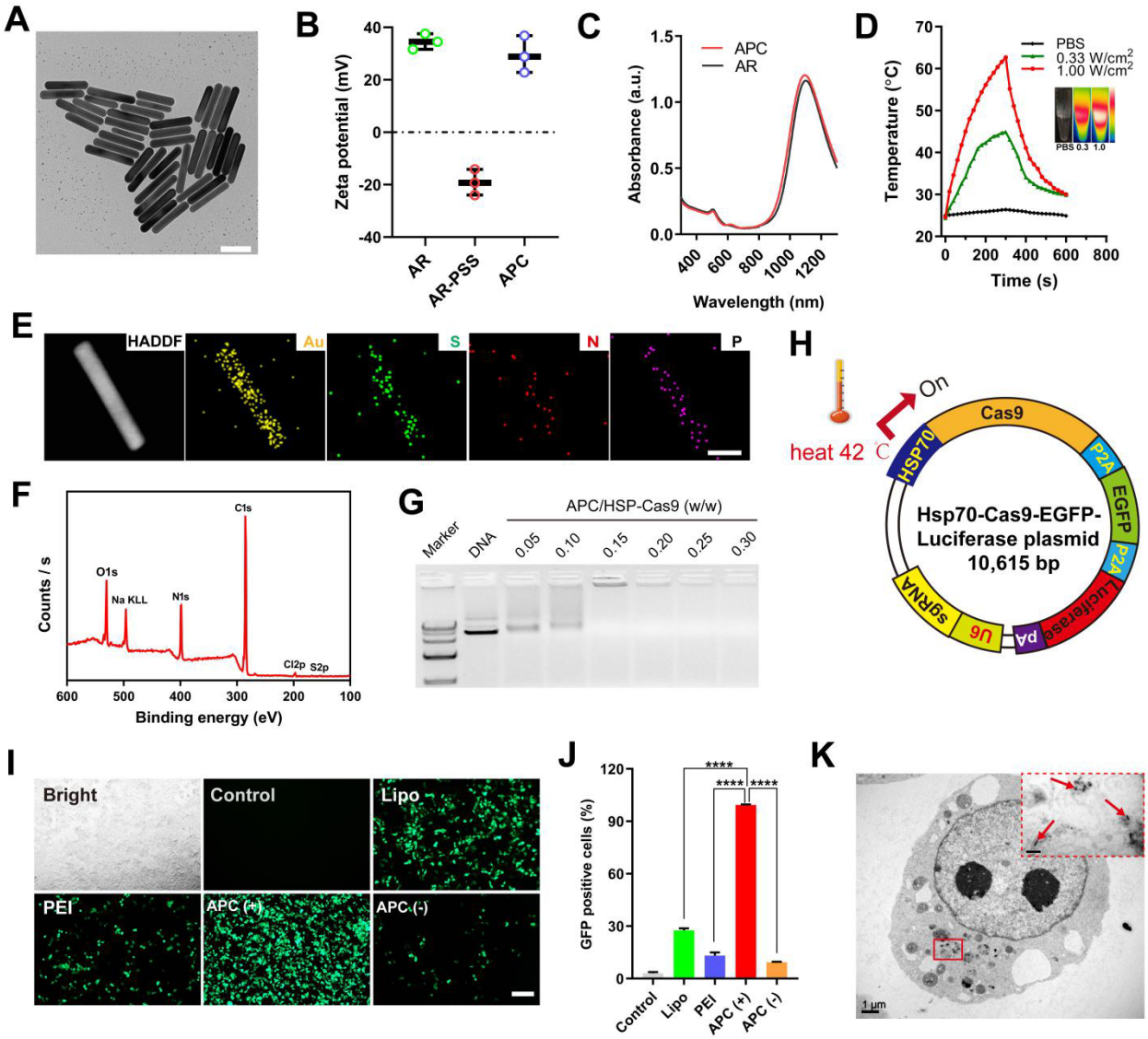


**Fig. 2**. Characterization of APC and evaluation of transfection activity. (A) TEM image of APC. (B) Zeta potential analysis of gold nanorods (AR), PSS-coated AR, and APC. Mean ± S.D., n = 3. (C) Absorption spectrum of AR and APC. (D) Solution temperature of APC as a function of laser irradiation time. The laser wavelength was 1064 nm. Insert, thermal image of PBS solution at a

laser power density of 0.33 W/cm$^2$ (left), APC solution at a power density of 0.33 W/cm$^2$ (middle), and 1.00 W/cm$^2$ (right) at their respective maximum temperature. (E) HADDF-STEM and EDS mapping of APC/HSP-Cas9. The scale bar indicates 25 nm. (F) XPS spectra of APC/HSP-Cas9 complexes. g. Agarose gel electrophoresis of APC/HSP-Cas9 complexes at various APC/DNA weight ratios. (H) HSP70 promoter-driven CRISPR/Cas9 plasmid (HSP-Cas9). The plasmid consists of a Cas9 gene driven by a HSP70 promoter, an EGFP reporter and a luciferase reporter downstream of Cas9, separated by self-cleaving peptides P2A. A segment of independent sgRNA sequence which is driven by U6 promoter was further inserted in the downstream of luciferase reporter. (I) GFP expression mediated by APC/HSP-Cas9 with (+) or without (-) laser irradiation at 1064 nm. Lipo- and PEI-mediated transfections at 42 °C were used as positive controls, whereas cells without any treatment were used as a negative control. The scale bar represents 200 µm. (J) Flow cytometry analysis of GFP-positive cells. Mean ± S.D., n = 3, *** $P < 0.001$. k. Bio-TEM image of 293T cells after the transfection of APC/HSP-Cas9 complexes. The arrows in the image show the presence of APC in the cytoplasm.

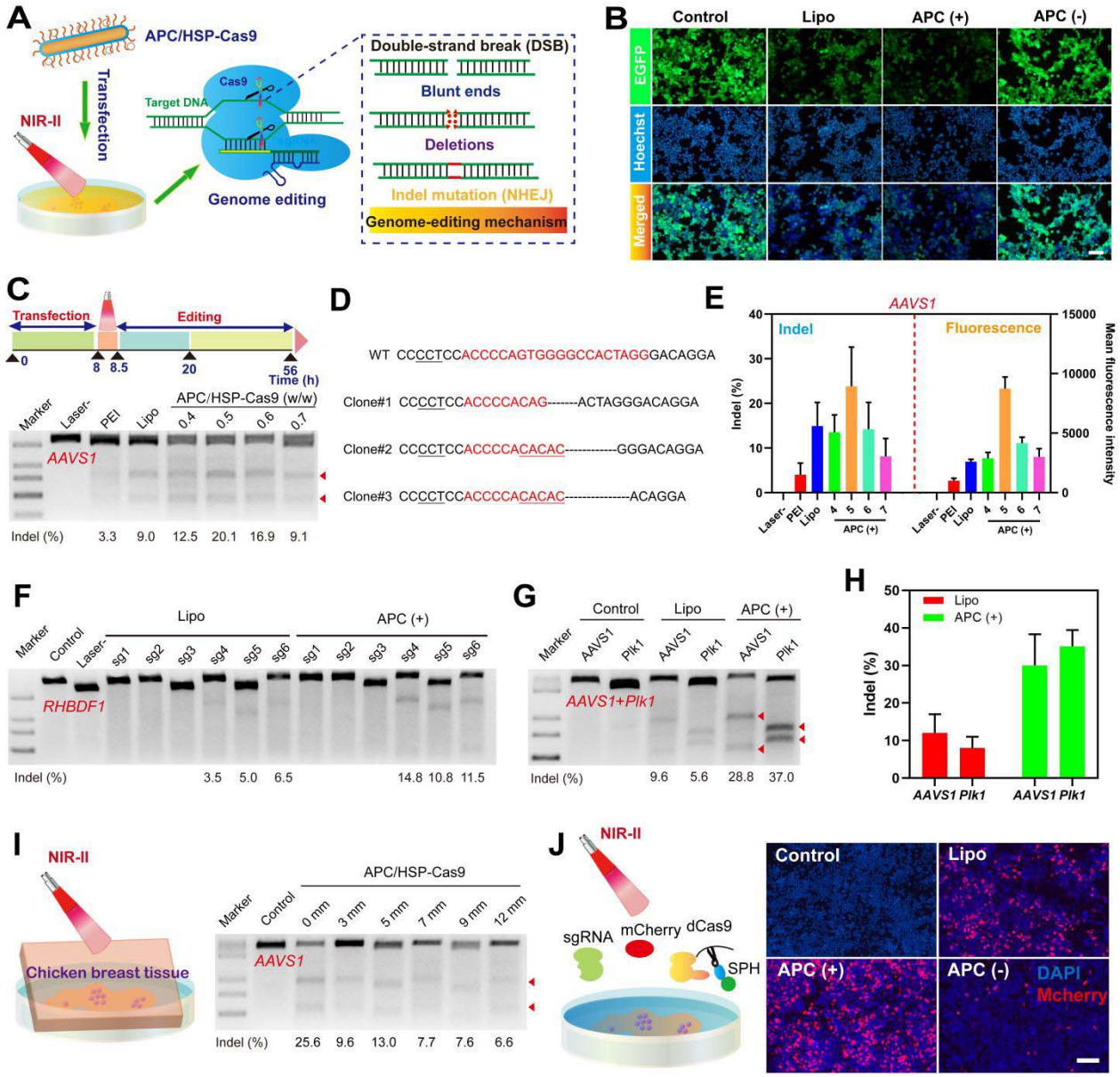


**Fig. 3.** Optogenetic activation of CRISPR/Cas9 genome editing by APC/HSP-Cas9. (A) Illustration of optogenetic activation mediated by APC. (B) CLSM images of 293T-EGFP cells treated with APC/HSP-Cas9 targeting EGFP, followed by optogenetic activation. Lipo-mediated transfection at 42 °C and APC-mediated transfection without irradiation were used as controls. The scale bar represents 200 μm. (C) Indel mutations of *AAVS1* locus of 293T cells transfected APC/HSP-Cas9 complexes with or without laser irradiation. APC was complexed with HSP-Cas9 at different weight ratios. Lipo and PEI were used as positive controls. (D) Sanger sequencing results of T-A cloning from 293T cells (*AAVS1*) after APC-mediated transfection and optogenetic activation. The target sequences were marked in red. PAM was underlined (black). Substitutions, insertions and deletions were marked by red base sequences, underlines (red), and dotted lines, respectively. (E) Analysis of indel rate, as revealed by the grayscale density of cut bands from T7E1 results, after the transfection of ACP/HSP-Cas9 targeting *AAVS1* with or without laser treatment (left panel). The corresponding GFP expression was evaluated. 4, 5, 6, and 7 refer to APC/HSP-Cas9 weight ratio 0.4, 0.5, 0.6 and 0.7, respectively. Mean ± S.D., n = 3. (F) Indel

mutations from 293T cells transfected APC/HSP-Cas9 targeting *RHBDF1* with or without laser irradiation. (G) Indel mutation from multiplex genome editing by ASP/HSP-Cas9 targeting *Plk1* and *AAVS1* with the laser irradiation. (H) Quantitative analysis of indel mutations after the multiplex editing at *Plk1* and *AAVS1* loci after the transfection of APC/HSP-Cas9 and optogenetic activation in 293T cells. Mean ± S.D., n = 3. (I) Illustration of cultured cells exposed to the irradiation in the presence of a piece of chicken breast tissue (left). Indel mutations of *AAVS1* locus from 293T transfected with APC/HSP-Cas9, followed by the irradiation in the presence of the breast chicken tissue of different thickness (right). (J) Illustration of optogenetic regulation of transcriptional activation *in vitro* (left). Optogenetic activation of mCherry expression after the co-transfection of plasmids of HSP-dCas9-SPH, miniCMV-mCherry and U6-sgRNA by APC (right).